

THE STELLAR INITIAL MASS FUNCTION IN PRIMORDIAL GALAXIES

FUMITAKA NAKAMURA

Faculty of Education and Human Sciences, Niigata University, 8050 Ikarashi-2, Niigata 950-2181, Japan, and
Astronomy Department, University of California, Berkeley, Berkeley, CA 94720

AND

MASAYUKI UMEMURA

Center for Computational Physics, University of Tsukuba, Tsukuba, Ibaraki 305-8577, Japan

Draft version November 18, 2018

ABSTRACT

In the context of star formation through fragmentation of an extremely metal-deficient protogalactic cloud, the gravitational collapse of filamentary gas clouds is explored with one-dimensional numerical hydrodynamics coupled with non-equilibrium chemistry of H₂ and HD. It is found that the cloud evolution is governed mainly by the initial central density ($n_{c,0}$) and H₂ abundance ($x_{\text{H}_2,0}$). In particular, the evolution of low-density filaments ($n_{c,0} \lesssim 10^5 \text{ cm}^{-3}$) bifurcates at a threshold H₂ abundance of $x_{\text{H}_2,\text{cr}} \simeq 3 \times 10^{-3}$, beyond which HD cooling overwhelms H₂ cooling. The contraction of a filament with $n_{c,0} \lesssim 10^5 \text{ cm}^{-3}$ and $x_{\text{H}_2,0} \gtrsim x_{\text{H}_2,\text{cr}}$ is strongly decelerated when the central density (n_c) reaches a critical density of HD at which LTE level populations are achieved, and therefore the filament is expected to fragment at $\sim 10^7 \text{ cm}^{-3}$. The fragment mass is assessed to be $\approx 10M_\odot$. In contrast, the contraction of a filament with $n_{c,0} \lesssim 10^5 \text{ cm}^{-3}$ and $x_{\text{H}_2,0} \lesssim x_{\text{H}_2,\text{cr}}$ is regulated by H₂ cooling. In this case, the filament tends to fragment at lower density as $\sim 10^4 \text{ cm}^{-3}$ owing to the low critical density of H₂, and the fragment mass is as high as $\approx 10^2M_\odot$. For a high-density filament with $n_{c,0} \gtrsim 10^5 \text{ cm}^{-3}$, the temperature stays at a relatively high value because both H₂ and HD cooling saturate, and the cloud evolution is governed by H₂ cooling. The contraction of a high-density filament is accelerated by effective three-body H₂ formation when the density reaches 10^{8-9} cm^{-3} . The fragmentation is not expected to take place until the cloud becomes opaque in H₂ lines at $n_{c,0} \sim 10^{12-13} \text{ cm}^{-3}$, so that the fragment mass is reduced to $1 - 2 M_\odot$. As a result, the stellar initial mass function (IMF) could be bimodal and deficient in sub-solar mass stars, where the high mass peak is around $10M_\odot$ or 10^2M_\odot , dependently on $n_{c,0}$ and $x_{\text{H}_2,0}$. If the protogalactic clouds are ionized by UV radiation or strong shocks, the H₂ abundance could exceed $x_{\text{H}_2,\text{cr}} \simeq 3 \times 10^{-3}$ by reactions of $\text{H} + \text{e} \rightarrow \text{H}^- + h\nu$ and $\text{H} + \text{H}^- \rightarrow \text{H}_2 + \text{e}$. The high mass peak would then be $O(10)M_\odot$.

Subject headings: cosmology: theory — galaxies: formation — hydrodynamics — ISM: clouds — stars: formation

1. INTRODUCTION

The first generation of stars, Population III stars, are thought to form from almost metal-free gas with metallicity of $\sim 10^{-10}Z_\odot$ (see e.g., Carr, Bond, & Arnett 1984; Carr 1994). Such Population III stars may have produced heavy elements at redshifts $z \gtrsim 10$. Recent observations of quasar absorption spectra show that the metal abundance in intergalactic space is $\approx 10^{-3}Z_\odot$ (e.g., Cowie & Songaila 1998). Also, it is widely accepted that a significant portion of old halo stars in our Galaxy have metallicity lower than $10^{-3}Z_\odot$ (Beers, Preston, & Shectman 1992). In addition, some blue compact dwarf galaxies are known to be extremely metal-poor ($\approx 10^{-2}Z_\odot$, Kunth & Sargent 1986; Pustilnik et al. 2001). Thus, star formation in protogalaxies must have proceeded in very metal-deficient environments.

When the metallicity is lower than $Z \lesssim 10^{-2}Z_\odot$, the cooling by heavy elements is less effective than cooling by hydrogen and helium (e.g., Yoshii & Sabano 1980; Böhringer & Hensler 1989; Omukai 2000; Nishi & Tashiro 2000). For the formation of Population III stars from such metal-deficient gas, the cooling by primordial hydrogen molecules (H₂) plays an essential role (Matsuda,

Sato, & Takeda 1969; Yoneyama 1972; Hutchins 1976; Silk 1977; Yoshii & Sabano 1980; Carlberg 1981; Lepp & Shull 1984; Palla, Salpeter, & Stahler 1983; Yoshii & Saio 1986; Shapiro & Kang 1987; Uehara et al. 1996; Haiman, Thoul & Loeb 1996; Nishi et al. 1998; Abel et al. 1998; Bromm, Coppi, & Larson 1999; Abel, Bryan, & Norman 2000; Nakamura & Umemura 1999a, 2001, hereafter Papers I and II). Recent studies have revealed that star formation in primordial gas is considerably different from present-day star formation, implying that the stellar initial mass function (IMF) might be different from the Salpeter-like IMF and the IMF might be time-varying in the course of galaxy evolution from the early collapsing stages to the present day (see also Larson 1998; Zepf & Silk 1996; Chabrier 1999).

Besides hydrogen molecules, deuterated hydrogen molecules (HD) can be a significant coolant (e.g., Galli & Palla 1998). Although HD is less abundant than H₂ ($[\text{HD}/\text{H}_2] \sim 10^{-3} - 10^{-4}$), HD has a finite dipole moment and thus higher radiative transition probabilities than H₂. For example, the lowest rotational transitions of H₂ and HD have radiative transition probabilities of $A_{20} = 3 \times 10^{-11} \text{ s}^{-1}$ and $A_{10} = 5 \times 10^{-8} \text{ s}^{-1}$, respectively.

Also, the corresponding excitation energies of H₂ and HD are $\Delta E_{20}/k = 510$ K and $\Delta E_{10}/k = 128$ K, respectively, where k is the Boltzmann coefficient. Thus, HD can lower the gas temperature down to $T \lesssim 100$ K (e.g., Puy & Signore 1996; Bougleux & Galli 1997; Galli & Palla 1998; Flower et al. 2000).

The first pregalactic objects should have collapsed at redshifts of $z \sim 10 - 10^2$ and have masses of $10^5 - 10^8 M_\odot$ in a cold dark matter cosmology (Tegmark et al. 1998; Fuller & Couchman 2000). When such first objects are virialized and the gas temperature ascends to $10^3 - 10^4$ K, H₂ formation is promoted and the fractional abundance is raised to $x_{\text{H}_2} = 10^{-4} - 10^{-3}$. However, for this H₂ abundance, the H₂ cooling cannot lower the temperature down to 100 K. Thus, the cloud evolution is basically controlled by H₂ cooling and HD cooling is not important (Nakamura & Umemura 1999b, 2000; see also Lepp & Shull 1984).

But, in some situations, the H₂ abundance can be raised further. Ferrara (1998) argued that in dense shells formed behind supernova shocks, H₂ molecules form efficiently owing to reduced recombination of free electrons (see also Shapiro & Kang 1987). In the dense shells, the H₂ concentration reaches 6×10^{-3} , and consequently the gas temperature descends to ~ 100 K. At such low temperature, HD is a more efficient coolant than H₂. The primordial star formation regulated by HD cooling in shocked shells is studied by several authors (Uehara & Inutsuka 2000; Machida, Fujimoto, & Nakamura 2001). Another possibility is star formation from photoionized gas. Corbelli, Galli, & Palla (1998) studied the effects of UV background radiation on the thermal evolution of the protogalaxies (see also Murray & Lin 1989; Haiman, Rees, & Loeb 1996). They found that at redshifts lower than $z \sim 1 - 2$, protogalactic clouds are self-shielded against the UV background radiation, and H₂ formation is promoted up to $x_{\text{H}_2} \approx 10^{-2}$ with the help of abundant free electrons due to the UV radiation. Even at higher redshifts ($z \gtrsim 2$), if pregalactic clouds more massive than $10^{11} M_\odot$ collapse under a UV background, they can be eventually self-shielded and abundant H₂ ($\gtrsim 10^{-3}$) forms, so that the temperature descends down to ~ 100 K (Susa & Umemura 2000). Hence, HD cooling is likely to be important for the star formation in the protogalactic systems. In this paper, we extensively examine the effects of the HD cooling on the formation of stars in protogalaxies, and elucidate the role of HD molecules for the stellar initial mass function (IMF) there.

This paper is organized as follows. In §2, we describe model and numerical methods which are basically the same as those of Paper II. Numerical results are presented in §3. In §4, implications for the IMF of Population III and metal-deficient stars are discussed.

2. MODEL AND NUMERICAL METHODS

In Papers I and II, we studied the fragmentation of filamentary clouds by incorporating the H₂ cooling. In this paper, we examine the effects of HD cooling on the evolution of the filaments. Our numerical model and method are the same as those of Paper II except for the inclusion of deuterium chemistry. In the following, we briefly review our numerical model. See §2 of Paper II for more detail.

We deal with the following 14 species: e, H, H⁺, H⁻, H₂, H₂⁺, He, He⁺, He⁺⁺, D, D⁺, D⁻, HD, and HD⁺. The mass

fraction of He is set to 0.24 of the total mass. The D abundance is set to 4×10^{-5} by number, which is consistent with recent observations of the deuterium Ly- α feature in the absorption spectra of high-redshift quasars (e.g., Tytler et al. 1996; O’Meara et al. 2000). The reaction rate coefficients for the deuterium chemistry are given in Table 1, while the rate coefficients for other species are the same as those of Paper II.

We take into account the following thermal processes: (1) H cooling by radiative recombination, collisional ionization, and collisional excitation, (2) H₂ line cooling by rotational and vibrational transitions, (3) cooling by H₂ collisional dissociation, (4) heating by H₂ formation, and (5) HD line cooling by rotational transitions.

The HD line cooling is computed by the same method as the H₂ line cooling described in Paper II, which includes the escape probability method in an optically-thick regime. For the collisional deexcitation rates for HD, we consider both H-HD and H₂-HD collisions, using analytical fits of Galli & Palla (1998) and Flower & Roueff (1999). The first 6 rotational levels are taken into account. Recently, Flower et al. (2000) derived an updated HD cooling function in an optical thin regime, which includes up to 8 rotational levels. We have checked the difference by employing their cooling function for several models described in §3, and found that the resultant temperatures agree with the present results to within $\sim 4\%$.

We consider an infinitely long cylindrical gas cloud which collapses in the radial direction. The initial temperature is assumed to be spatially constant. The initial abundances of electron and D⁺ are set to $x_e = 5 \times 10^{-5}$ and $x_{\text{D}^+} = 1 \times 10^{-7}$, respectively. (The numerical results do not depend sensitively upon x_e and x_{D^+} . See also §2 of Papers I and II.) At the initial state, the relative abundances of H⁻, H₂⁺, He⁺, He⁺⁺, D⁻, HD, and HD⁺ are set to zero for simplicity. The abundances of other species are determined by the conservation of mass and charge. The initial density profile in the radial direction is assumed to be

$$\rho_0 = \rho_{c,0} (1 + r^2/R_0^2)^{-2}, \quad (1)$$

where $R_0 = \sqrt{2fkT_0/(\pi G\rho_{c,0}\mu)}$ is the effective radius, $\rho_{c,0}$ is the central mass density, T_0 is the initial gas temperature, μ is the mean molecular weight, and f is the ratio of the gravitational force to the pressure force. When $f = 1$, the density distribution agrees with that of an isothermal cylinder in hydrostatic equilibrium. When the filamentary cloud forms through gravitational fragmentation of a parent sheet-like cloud, f is expected to be ≈ 2 (see §2.2 of Paper I). The radial infall velocity is given by

$$v_{r,0} = -v_0 r \left(R_0 + \sqrt{R_0^2 + r^2} \right)^{-1}, \quad (2)$$

where v_0 is constant and is set to the initial sound speed. We neglect the effects of dark matter because after virialization of the parent system, the local density of baryonic gas is likely to be higher than the background dark matter density owing to radiative cooling (e.g., Umemura 1993). The model is thus specified by four parameters: $n_{c,0}$, T_0 , f , and the initial H₂ fractional abundance $x_{\text{H}_2,0}$. As stated in §1, high H₂ abundance as $x_{\text{H}_2,0} \gtrsim 10^{-3}$ can be achieved if a parent cloud undergoes ionization prior to the collapse.

In Paper II, we followed the collapse and fragmentation of the primordial filaments with one-dimensional and two-dimensional axisymmetric simulations. The numerical results of Paper II showed that the fragment masses derived from the two-dimensional simulations are in good agreement with the estimate based on one-dimensional simulations. Therefore, in this paper, we pursue one-dimensional simulations on the collapse of the filaments to estimate the fragment masses.

We calculated more than 3000 models by choosing the model parameters $n_{c,0}$, T_0 , f , and $x_{\text{H}_2,0}$ as $\log_{10}(n_{c,0}/\text{cm}^{-3}) = 1.00, 1.33, 1.67, 2.00, \dots, 6.00$, $T_0 = 200, 300, 400$ K, $f = 1.5, 2.0, 2.5, \dots, 6.0$, and $x_{\text{H}_2,0} = 1 \times 10^{-4}, 3 \times 10^{-4}, 6 \times 10^{-4}, 1 \times 10^{-3}, \dots, 1 \times 10^{-2}$, respectively.

3. NUMERICAL RESULTS

In Papers I and II, we studied the fragmentation of the primordial filaments incorporating H_2 cooling, and it was shown that the fragmentation is bifurcated by a threshold initial density of $\approx 10^5 \text{cm}^{-3}$, below which as massive stars as $\approx 10^2 M_\odot$ form, and above which less massive stars with $\approx 1 M_\odot$ form.

In this section, we reexamine the collapse of the filaments, including the HD cooling as well as H_2 cooling. As shown below, there is a threshold initial H_2 concentration, above which HD cooling predominantly regulates the cloud evolution. We also show that the HD cooling does not play an important role for high-density gas. Thus, the evolution of the filaments is classified into three cases, depending upon the initial density, $n_{c,0}$, and initial H_2 abundance, $x_{\text{H}_2,0}$; (1) low-density filaments with high $x_{\text{H}_2,0}$, (2) low-density filaments with low $x_{\text{H}_2,0}$, and (3) high-density filaments.

In the following, we first compare the HD cooling and H_2 cooling on the $n_{c,0}-x_{\text{H}_2,0}$ diagram to clarify the importance of HD cooling. Next, we show the numerical results of one-dimensional simulations. In the models shown in this section, the initial temperatures are set to be equilibrium temperatures of the filaments which decrease with increasing $x_{\text{H}_2,0}$.

3.1. Threshold H_2 Abundance

HD cooling depends sensitively on the initial cloud density and H_2 abundance. To clarify the effect of HD cooling, we compare the HD cooling rate (Λ_{HD}) and the H_2 cooling rate (Λ_{H_2}) in Figure 1. The abscissa and ordinate indicate the initial gas density and the H_2 abundance, respectively. The solid lines show the contour curves of the HD-to- H_2 cooling ratio ($\Lambda_{\text{HD}}/\Lambda_{\text{H}_2}$). When evaluating the cooling rates, the gas temperatures are determined iteratively to satisfy the condition of $t_{\text{cool}} = t_{\text{frag}}$, where t_{cool} is cooling time and t_{frag} is fragmentation time as defined in §3.2. The resultant temperatures are also shown by dashed lines. The HD abundance is taken to be proportional to the H_2 abundance as $x_{\text{HD}}/x_{\text{H}_2} = 1 \times 10^{-4}$, which is consistent with those in the models shown in §3.3 and 3.4. This figure shows that the contribution of HD cooling rate is largest around $n_{c,0} = 10^5 \text{cm}^{-3}$, which is almost comparable to the critical density of HD, beyond which the rotational level populations achieve the LTE.

If the cloud has the initial H_2 abundance lower than a

threshold value of $x_{\text{H}_2,\text{cr}} = 3 \times 10^{-3}$, HD cooling does not play a significant role in the thermal evolution of the cloud because $\Lambda_{\text{HD}} < \Lambda_{\text{H}_2}$. The cloud temperature is then equal to the equilibrium temperature shown by the dashed lines. As shown later, the H_2 abundance in a collapsing filament stays almost constant before the three-body reactions proceed at 10^{8-9}cm^{-3} . Thus, if an evolutionary path of such a cloud is superimposed on Figure 1, then it is almost parallel to the abscissa. For the filaments with $n \lesssim 10^5 \text{cm}^{-3}$ and $x_{\text{H}_2} \gtrsim x_{\text{H}_2,\text{cr}}$, the evolutionary path enters into the region of $\Lambda_{\text{HD}} > \Lambda_{\text{H}_2}$ in the course of contraction even if Λ_{H_2} is larger than Λ_{HD} at the initial state. In actual evolution, as shown below, the pressure force retards the contraction of the filament. In particular, when the density exceeds HD critical density, $n_{\text{HD,cr}} \sim 10^{4-5} \text{cm}^{-3}$, the contraction slows and the actual cloud temperature stays below 100 K. Consequently, HD cooling continues to control the contraction until the cloud becomes opaque to the HD lines. On the other hand, for the filaments with $n_{c,0} \gtrsim 10^5 \text{cm}^{-3}$ and $x_{\text{H}_2,0} \gtrsim x_{\text{H}_2,\text{cr}}$, the evolutionary path goes into the region of $\Lambda_{\text{HD}} < \Lambda_{\text{H}_2}$ even if Λ_{HD} is larger than Λ_{H_2} at the initial state. As a result, for the initial condition in the gray region in Figure 1, the HD cooling plays an important role in the thermal evolution of the gas.

3.2. Low-Density Filaments with high H_2 abundance ($n_{c,0} \lesssim 10^5 \text{cm}^{-3}$ and $x_{\text{H}_2,0} \gtrsim 3 \times 10^{-3}$)

As a typical example in which the HD cooling controls the contraction, we show the evolution of the model with $n_{c,0} = 10 \text{cm}^{-3}$, $T_0 = 200$ K, $f = 2$, and $x_{\text{H}_2,0} = 3 \times 10^{-3}$.

Figures 2a, 2b, 2c, and 2d show the time evolution of (a) the temperature, (b) H_2 (*solid line*) and HD (*dashed line*) abundances, (c) cooling rates by H_2 (*dashed line*) and by HD (*dotted line*), and the total (*solid line*), (d) the cooling timescale (*solid line*), the timescale of dynamical contraction (*dashed line*), and the fragmentation timescale (*dotted line*), respectively, as a function of the central density [$n_c \equiv \rho_c/(\mu m_H)$]. Since the central density monotonically increases with time, the abscissa corresponds to the evolution time. The contraction and cooling timescale are, respectively, defined as $t_{\text{dyn}} \equiv \rho/\dot{\rho}$ and $t_{\text{cool}} \equiv E_t/(\Lambda_t)$, where E_t and Λ_t are total internal energy and net cooling rate, respectively. The fragmentation time, t_{frag} , is defined as 2.5 times the inverse of the growth rate of the fastest-growing mode (eq [38] of Nakamura, Hanawa, & Nakano 1993), i.e., $t_{\text{frag}} \equiv 5.17(2\pi G\rho)^{-1/2}$. Note that this definition of t_{frag} is 2.5 times larger than that of Paper II. In practice, a filament does not fragment in one-dimensional calculations. Therefore, t_{frag} should be regarded as a measure of the fragmentation epoch as well as the free-fall time-scale.

At the early stages of the contraction, H_2 cooling dominates HD cooling, and the equilibrium temperature is lowered to $T \sim 100$ K owing to the high H_2 abundance. When the density reaches the critical density of H_2 , $n_{\text{H}_2,\text{cr}} \sim 10^{3-4} \text{cm}^{-3}$, the H_2 cooling is saturated and then HD cooling becomes dominant as the density increases. When the HD cooling becomes effective, the equilibrium temperature descends to ~ 50 K owing to the lower excitation temperatures of HD. Thereafter, the temperature stays nearly constant at ~ 50 K during the contraction. When the density reaches $n_{\text{HD,cr}} \sim 10^{4-5} \text{cm}^{-3}$, the cloud

contraction tends to become quasistatic by the combination effect of (1) the dynamical stability of a *cylindrical* cloud and (2) the characteristic of line cooling. First, a polytropic cylinder in hydrostatic equilibrium with $P \propto \rho^\gamma$ is gravitationally stable in the radial directions, if the effective γ is greater than unity. This means that an isothermal cylinder is marginally stable. Second, at lower density than the critical density, the line cooling rate is nearly proportional to n^2 because the collisional excitation rate balances with spontaneous emission rate, while at higher density than the critical density, the cooling rate is proportional to n because the level populations reach LTE. Hence, t_{cool} is inversely proportional to the density for $n < n_{\text{HD,cr}}$, while t_{cool} is constant for $n > n_{\text{HD,cr}}$ if the temperature is constant. By these effects, the compressional heating strongly brakes the dynamic contraction when $n > n_{\text{HD,cr}}$ and then the cloud evolves quasistatically.

When the density reaches $\sim 10^9 \text{ cm}^{-3}$, the cloud becomes optically thick in the HD lines and the quasistatic contraction almost ceases. However, before the central density reaches this density, the filament is likely to fragment. As shown by two-dimensional calculations in Paper II, it is anticipated that the fragmentation takes place when the dynamical timescale becomes a few times longer than the fragmentation timescale (see Paper II for more detail). From Figure 2d, this cloud is expected to undergo the fragmentation when the density reaches 10^7 cm^{-3} .

Uehara & Inutsuka (2000) estimated the minimum fragment mass when the HD lines become opaque. However, in their model, the cloud becomes optically thick to the HD lines when the density reaches $\approx 3 \times 10^{10} \text{ cm}^{-3}$, which is about 30 times higher than the present result. To understand this discrepancy, we compare our evaluation of the optical depth with the LVG approximation (Goldreich & Kwan 1974) with some modification. The optical depth of the LVG approximation is originally given by

$$\tau_{J+1,J} = \frac{hc}{4\pi} \frac{B_{J,J+1} n_J}{|dv/ds|} \left(1 - \frac{g_J n_{J+1}}{g_{J+1} n_J} \right), \quad (3)$$

where h is the Planck constant, c is the speed of light, $B_{J,J+1}$ is Einstein's B coefficient of the transition $J \rightarrow J+1$, $|dv/ds|$ is the velocity gradient, n_J and g_J are the number density and the Gaunt factor of the J level, respectively. However, in the present calculations, the velocity gradient is small compared to the thermal width and the gradient of the thermal velocity is dominant. Hence, we replace the velocity gradient by $\alpha v_{\text{th}}/R_J = \alpha \sqrt{\pi G \rho_c}$, where α , v_{th} , and R_J are a nondimensional numerical constant, the thermal velocity, and the filament radius, respectively. If we set the temperature to 60 K, the optical depth of the most effective cooling line ($J = 1 \rightarrow 0$) becomes unity when the density reaches $1 - 3 \times 10^9 \text{ cm}^{-3}$ for $\alpha = 1 - 2$. This is consistent with the present result. Also, it should be noted that our definition of the fragment mass is different from that of Uehara & Inutsuka (2000). We adopt the mass contained within one wavelength of the fastest-growing linear perturbation which is consistent with our two-dimensional numerical results (see §4), while Uehara & Inutsuka (2000) adopted the Jeans mass which is about ten times smaller than our definition at the same density and temperature. As a result, their estimation of the fragment mass is by about two orders of magnitude smaller

than our estimate if we assume the cloud to fragment at the stage optically thick to the HD lines. However, in practice, the cloud is likely to fragment at the earlier stages around the critical density of HD as shown above.

The evolution of the other models with different initial parameters ($10 \text{ cm}^{-3} \lesssim n_{c,0} \lesssim 10^4 \text{ cm}^{-3}$, $200 \text{ K} \lesssim T_0 \lesssim 400 \text{ K}$, $1.5 \lesssim f \lesssim 6$, and $3 \times 10^{-3} \lesssim x_{\text{H}_2,0} \lesssim 10^{-2}$) is qualitatively similar to that of the model shown in Figure 2. When the initial H_2 abundance is as high as 10^{-2} , the HD cooling is more effective than H_2 cooling at the initial state. Thus, the temperature goes down to $\sim 50 \text{ K}$ at the very early stages of the evolution.

3.3. Low-Density Filaments with Low H_2 Abundances ($x_{\text{H}_2,0} \lesssim 3 \times 10^{-3}$)

As a typical example of this case, we show the evolution of the model with $n_{c,0} = 10 \text{ cm}^{-3}$, $T_0 = 400 \text{ K}$, $f = 2$, and $x_{\text{H}_2,0} = 1 \times 10^{-4}$ in Figure 3. The notation of the figure is the same as that of Figure 2.

In this model, $\Lambda_{\text{HD}} < \Lambda_{\text{H}_2}$ during the contraction, and thus HD cooling does not play a significant role in the thermal and dynamical evolution. The temperature remains between 100 and 500 K over 11 orders of magnitude in density until the H_2 lines become optically thick. During the contraction, the HD abundance is nearly proportional to that of H_2 ($x_{\text{HD}} \sim 10^{-4} x_{\text{H}_2}$) because HD molecules form primarily via the reaction $\text{D} + \text{H}_2 \rightarrow \text{H} + \text{HD}$. Thus, when the three-body H_2 formation becomes effective, almost all the D atoms are processed into HD. It should be noted that the above reaction is sensitive to the temperature, and for lower temperature, the reactions $\text{D}^+ + \text{H}_2 \rightarrow \text{H}^+ + \text{HD}$ and $\text{HD}^+ + \text{H} \rightarrow \text{D}^+ + \text{HD}$ are more effective.

The contraction proceeds quasistatically after the density reaches the critical density of H_2 ($n_{\text{H}_2,\text{cr}} = 10^{3-4} \text{ cm}^{-3}$). When the three-body H_2 formation becomes effective, the contraction is accelerated again and then decelerated when the cloud becomes optically thick to the H_2 lines ($n_c \sim 10^{12} \text{ cm}^{-3}$). The cloud is expected to fragment after the density reaches the critical density of H_2 .

The evolution of the other models with different parameters ($10 \text{ cm}^{-3} \lesssim n_{c,0} \lesssim 10^4 \text{ cm}^{-3}$, $200 \text{ K} \lesssim T \lesssim 400 \text{ K}$, $1.5 \lesssim f \lesssim 6$, and $10^{-4} \lesssim x_{\text{H}_2,0} \lesssim 10^{-3}$) is qualitatively similar to that of this model.

3.4. High-Density Filaments

As a typical example of this case, we show the evolution of the model with $n_{c,0} = 10^6 \text{ cm}^{-3}$, $T_0 = 200 \text{ K}$, $f = 6$, and $x_{\text{H}_2,0} = 1 \times 10^{-2}$ in Figure 4. The notation of the figure is the same as that of Figure 2.

Although the initial H_2 abundance is as high as the threshold H_2 abundance 3×10^{-3} , the evolution is essentially the same as those of the models with low $x_{\text{H}_2,0}$ (see §3.2 of Paper II). Since $n_{c,0}$ is already higher than $n_{\text{H}_2,\text{cr}}$ and $n_{\text{HD,cr}}$, the temperature increases as the collapse proceeds. Therefore, even if HD cooling is more effective than H_2 cooling at the initial state, H_2 cooling becomes dominant as the collapse proceeds. In other words, the evolution is essentially the same as that without HD cooling.

The contraction time does not become longer than the fragmentation time until the H_2 lines become optically thick ($n_c \sim 10^{12} \text{ cm}^{-3}$) due to the rapid increase in the H_2

abundance via the effective three-body reactions. Therefore, the fragmentation is not expected to take place until the cloud becomes opaque to the H₂ lines.

The evolution of the other models with different parameters ($n_{c,0} \gtrsim 10^5 \text{ cm}^{-3}$, $200 \text{ K} \lesssim T \lesssim 400 \text{ K}$, $3 \lesssim f \lesssim 6$, and $10^{-4} \lesssim x_{\text{H}_2,0} \lesssim 10^{-2}$) is qualitatively similar to that of this model.

It is noted that for the high-density filaments with *low* f (e.g., $f \lesssim 2$ for $T_0 = 300 \text{ K}$), t_{dyn} becomes comparable to or longer than t_{frag} before n_c reaches 10^8 cm^{-3} . This is because when the parameter f is small (or the initial line mass is small), the equilibrium line mass of the filament, which is proportional to the temperature, approaches the total line mass of the cloud before the three-body reactions become significant. The contraction of such a cloud is decelerated significantly around $n_c \sim 10^8 \text{ cm}^{-3}$, and thus the cloud is likely to fragment around this density.

4. DEPENDENCE OF THE FRAGMENT MASS ON THE INITIAL MODEL PARAMETERS

In this section, we estimate the fragment masses with our numerical results. As shown above, there is a threshold H₂ abundance, beyond which the HD cooling can play a key role in the thermal evolution of primordial gas clouds, and also there is a threshold initial density, below which the filament would fragment at the critical density of H₂ or HD. Hence, as anticipated from the above numerical results, the fragment mass is also divided into three cases, depending upon the initial H₂ abundance and density.

Comparing one-dimensional results with the two-dimensional results shown in Paper II, we found that the fragmentation takes place when t_{dyn} reaches 2–3 times the inverse of the growth rate of the fastest-growing perturbation. We thus assume that a filament fragments into dense cores when the dynamical time reaches the fragmentation time, $t_{\text{dyn}} = t_{\text{frag}}$. The fragment masses are computed as $M_{\text{frag}} \equiv m_{\text{eff}} \lambda$, where $m_{\text{eff}} = \int 2\pi r \rho dr$ is a line mass which is obtained by integrating the density from the center to the radius at which the density takes $0.1n_c$ and λ is a longitudinal wavelength of a fastest-growing linear perturbation (eq.[38] of Nakamura et al. 1993). This mass is about ten times larger than the Jeans mass.

Figures 5a and 5b show the fragment mass for the models with $x_{\text{H}_2,0} = 1 \times 10^{-3}$ and 3×10^{-3} , with assuming equilibrium initial temperature. The abscissa and ordinate denote the initial central density and the parameter f , respectively. The solid lines denote the contours of the fragment mass with adjacent numbers in units of M_\odot . The thick dashed lines show the boundary at which the HD cooling rate is equal to H₂ cooling rate at the epoch of fragmentation. In the regions to the left of the dashed lines, HD cooling is more effective than H₂ cooling. Filamentary clouds are expected to form by the fragmentation of self-gravitating disks. According to numerical simulations, when the filaments form by the growth of the most unstable modes, their line masses tend to be twice the line mass for hydrostatic equilibrium, $\mu_{\text{eq}} \equiv 2c_s^2/G$, where c_s is a sound speed. For comparison, the line masses of the filaments with $1.5\mu_{\text{eq}}$, $2\mu_{\text{eq}}$, and $2.5\mu_{\text{eq}}$ are shown by dot-dashed lines. The line mass of the equilibrium filament depends only on the equilibrium temperature that is determined by the balance between the cooling time and the

fragmentation time of the self-gravitating disk. Here, the fragmentation time is defined as the inverse of the most unstable linear perturbation (see Larson 1985). The total line masses of the filaments are proportional to fT_0 . Therefore, the ordinate in Figure 5 corresponds to the total line masses of the filaments.

For the models with $x_{\text{H}_2,0} < x_{\text{H}_2,\text{cr}} \approx 3 \times 10^{-3}$ (Fig. 5a), the distribution of the fragment mass is quite similar to the case without HD (Paper II), because HD cooling does not play an important role in the thermal evolution of the filaments. For higher initial density and/or larger f , the fragment mass is lower. The maximum and minimum masses are estimated as $\sim 10^3 M_\odot$ and $1 - 2 M_\odot$, respectively. The former corresponds to the Jeans mass at the stage at which the density reaches a critical density of H₂. The latter corresponds to the Jeans mass at the stage at which the cloud becomes opaque to the H₂ lines. [The maximum mass is a few times smaller than that of Paper II because of the higher initial H₂ abundance. For the models with $x_{\text{H}_2,0} = 1 \times 10^{-4}$, the mass distribution as well as the maximum mass is in good agreement with that of Paper II. See Figure 1a of Nakamura & Umemura (2002).]

There is a steep boundary at $n_{c,0} \sim 10^4 - 10^5 \text{ cm}^{-3}$ in the distribution of the fragment mass for $f \gtrsim 3$. For the models with $n_{c,0} \gtrsim 10^5 \text{ cm}^{-3}$, the fragment masses take their minima at $1 \sim 2 M_\odot$, whereas, for the models with $n_{c,0} \lesssim 10^5 \text{ cm}^{-3}$, they are greater than $\sim 10^2 M_\odot$. This sensitivity in the fragment mass comes from the rapid increase in the H₂ abundance due to the three-body reactions. For the models with low densities ($n_{c,0} \lesssim 10^5 \text{ cm}^{-3}$), the contraction becomes quasistatic when the density reaches the critical density of H₂ and then linear density fluctuations can grow nonlinearly before the three-body H₂ formation becomes dominant ($n_{c,0} \gtrsim 10^{8-9} \text{ cm}^{-3}$). In contrast, for the models with high densities ($n_{c,0} \gtrsim 10^{5-6} \text{ cm}^{-3}$ and $f \gtrsim 3$), the contraction time does not exceed the fragmentation time until the H₂ lines become optically thick at $n \sim 10^{12} - 10^{13} \text{ cm}^{-3}$.

On the other hand, when the initial H₂ abundance is higher than 3×10^{-3} (Fig. 5b), the HD cooling is more effective than the H₂ cooling for low-density filaments. Thus, the maximum mass of the low-density region is reduced to a few tens M_\odot (The fragment mass depends weakly upon the initial H₂ abundance. For example, for the models with $x_{\text{H}_2,0} = 1 \times 10^{-2}$, the fragment mass is around $10 M_\odot$ in the low-density region.). The reduced maximum mass is then related to the Jeans mass at the stage at which the density reaches a critical density of HD. The minimum mass does not change because HD is not a dominant coolant in the evolution of dense filaments. Therefore, similarly to the models with low H₂ abundance, the dependence of the fragment mass on the initial density exhibits a steep boundary around $n_{c,0} = 10^4 - 10^5 \text{ cm}^{-3}$ for $f \gtrsim 3$.

As mentioned in §3.4, for the high density filaments with low f , the contraction time temporally becomes longer than the fragmentation time just before the three-body reactions become important. Thus, fragmentation is expected to take place before the three-body H₂ formation becomes efficient. As a result, the fragment masses are relatively large (the lower-right regions in Figure 5).

In summary, the distributions of the fragment mass has a steep boundary around $n_{c,0} \gtrsim 10^{4-5} \text{ cm}^{-3}$ for $f \gtrsim 3$, respectively of the initial H_2 abundance. This implies that the IMFs in very metal-deficient gas are likely to be bimodal if both low-density and high-density filaments form stars. The low-mass peak is around a few M_\odot , which is not sensitive to the abundance of H_2 formed in a parent cloud. The high-mass peak is $\approx 10^2 M_\odot$ if $x_{\text{H}_2,0} \lesssim 3 \times 10^{-3}$, while it is $\approx 10 M_\odot$ if $x_{\text{H}_2,0} \gtrsim 3 \times 10^{-3}$.

5. DISCUSSION

First, we briefly discuss the role of HD for the formation of the very first stars (Pop III stars). In the bottom-up scenarios like cold dark matter models, when the first pregalactic objects with masses of $10^5 - 10^8 M_\odot$ are virialized at redshifts of $z \sim 10 - 10^2$, the H_2 abundance reaches at most $10^{-4} - 10^{-3}$ which is lower than the threshold H_2 abundance. Therefore, the cloud evolution is basically determined by H_2 cooling rather than HD cooling (Nakamura & Umemura 1999b, 2000). If the primordial D abundance is a few times as high as the value we assumed ($x_{\text{D}} = 4 \times 10^{-5}$), HD cooling may play a role in the thermal evolution of the pregalactic clouds. However, recent observations of quasar absorption spectra find an observed primordial D abundance as low as $3 - 4 \times 10^{-5}$ (Tytler et al. 1996), implying that HD cooling is not important for the first star formation.

Next, we give some implications for star formation in metal-deficient primordial galaxies. Recently, Susa & Umemura (2000) investigated the pancake collapse of pregalactic clouds under UV background radiation. They found that once the pancake disk is shielded against external UV radiation in the course of contraction, H_2 molecules form efficiently via the H^- reaction with abundant free electrons produced by UV background, and the resultant abundance reaches $x_{\text{H}_2} \approx 3 \times 10^{-3}$ (see also Shapiro & Kang 1986). The pancake disks probably fragment into filaments in which stars can subsequently form. In this case, HD cooling is expected to become efficient in low-density filaments, and then the high mass peak of the IMF would go down to $\sim 10 M_\odot$.

It is found that at redshifts of $z \sim 2$, the UV background radiation decreases with time (Irwin, McMahon, & Hazard 1991; Maloney 1993). The time-decreasing UV

background radiation is likely to influence star formation in galaxies, especially low surface brightness galaxies (e.g., Ellis 1997). Corbelli et al. (1998) studied the effects of the declined UV background radiation on the thermal evolution of the protogalaxies with low surface densities. They found that there is a critical redshift of $z \sim 1 - 2$, above which the gas disks with surface densities $10^{20} \text{ cm}^{-2} \lesssim N_{\text{HI}} \lesssim 10^{21} \text{ cm}^{-2}$ are gravitationally stable at $T \sim 10^4 \text{ K}$. Below this redshift, the declined UV radiation is shielded by the gas disks where the H_2 abundance reaches 10^{-2} owing to high ionization degree by the UV radiation. Also, in such galaxies, the high mass peak of the IMF would decrease to $\sim 10 M_\odot$ owing to the HD cooling.

The high mass end of the IMF can influence abundance patterns because metal production by extremely metal-deficient stars is very different between $10^2 M_\odot$ and $10 M_\odot$ (Abia et al. 2001; Umeda & Nomoto 2001; Heger & Woosley 2001; Schaerer 2001). For instance, the abundance pattern in the metal-poor ($\sim 0.05 Z_\odot$) starburst galaxy M82 cannot be accounted for unless stars with $\gtrsim 25 M_\odot$ contribute significantly to the metal enrichment of the galaxy (Tsuru et al. 1997; Nakamura et al. 2001; Umeda & Nomoto 2001). This mass scale seems to be consistent with the high mass peak of the present IMF regulated by the HD cooling. It is also consistent with the estimate by Hernandez & Ferrara (2001).

As the star formation progresses, the interstellar metallicity will monotonously increase with time. When the metallicity reaches $10^{-3} - 10^{-2} Z_\odot$, the metal cooling becomes important and the thermal properties of the gas are changed. Thereafter, the process of star formation would become similar to the present-day case. In other words, the IMF would settle into Salpeter-like IMF.

We are grateful to A. Ferrara, T. Nakamoto, R. Nishi, K. Omukai, H. Susa, and H. Uehara for stimulating discussion. Numerical computations were carried out on VPP300/16R at the Astronomical Data Analysis Center of the National Astronomical Observatory, Japan and on workstations at the Center for Computational Physics, University of Tsukuba. This work was financially supported in part by the Grant-in-Aid for Scientific Research on Priority Areas of the Ministry of Education, Science, Sports and Culture 10147205 and 11134203 (FN).

REFERENCES

- Abel, T., Anninos, P. A., Norman, M. L., & Zhang, Y. 1998, *ApJ*, 508, 518
 Abel, T., Bryan, G. L., & Norman, M. L. *ApJ*, 540, 39
 Abia, C., Dominguez, I., Straniero, O., Linongi, M., Chieffi, A., & Isern, J. 2001, *ApJ*, 557, 126
 Beers, T. C., Preston, G. W., & Shtetman, S. A. 1992, *AJ*, 103, 1987
 Böhringer & Hensler, 1989, *ApJ*, 215, 147
 Bougleux, E., Galli, D., 1997, *MNRAS*, 638, 648
 Bromm, V., Coppi, P. S., Larson, R. B. 1999, *ApJ*, 527, L5
 Carlberg, R. G. 1981, *MNRAS*, 197, 1021
 Carr, B. J., Bond, J. R., & Arnett, W. D. 1984, *ApJ*, 277, 445
 Carr, B. J. 1994, *ARA&A*, 32, 531
 Chabrier, G. 1999, *ApJ*, 513, 103
 Corbelli, E., Galli, D., & Palla, F. 1997, *ApJ*, 487, L53
 Couchman, H. M. P., & Rees, M. J. 1986, *MNRAS*, 221, 53
 Cowie, L. L., & Songaila, A. 1998, *Nature*, 394, 44
 Ellis, R. S. 1997, *ARA&A*, 35, 389
 Ferrara, A. 1998, *ApJ*, 499, L17
 Flower, D. R. 2000, *MNRAS*, 318, 875
 Flower, D. R., Le Bourlot, J., Pineau des Forets, G., & Roueff, E. 2000, *MNRAS*, 314, 753
 Fuller, T. M., & Couchman, H. M. P. 2000, *ApJ*, 544, 6
 Galli, D., & Palla, F. 1998, *A&A*, 335, 403
 Goldreich, P. & Kwan, J. 1974, *ApJ*, 189, 441
 Haiman, Z., Rees, M. J., & Loeb, A. 1996, *ApJ*, 467, 522
 Haiman, Z., Thoul, A. A., & Loeb, A. 1996, *ApJ*, 464, 523
 Heger, A. & Woosley, S. E. 2001, submitted to *ApJ*(astro-ph/0107037)
 Hernandez, X. & Ferrara, A. 2001, *MNRAS*, in press
 Hutchins, J. B., 1976, *ApJ*, 205, 103
 Irwin, M., McMahon, R., & Hazard, C. 1991, *ASP Conf. Ser.* in *The Space Distribution of Quasars*, Vol. 21, 117
 Kunth, D., & Sargent, W. L. W. 1986, *ApJ*, 300, 496
 Larson, R. B. 1985, *MNRAS*, 214, 379
 Larson, R. B. 1998, *MNRAS*, 301, 569
 Lepp, S., & Shull, M. 1984, *ApJ*, 280, 465
 Machida, M., Fujimoto, M. Y. & Nakamura, F. 2001, in *The Physics of Galaxy Formation*, p. 355
 Maloney, P. 1993, *ApJ*, 414, 41

- Matsuda, T., Sato, H., & Takeda, H. 1969, *Prog. Theor. Phys.*, 42, 219
- Murray, S. D. & Lin, D. N. C. 1989, *ApJ*, 339, 933
- Nakamura, F., Hanawa, T., & Nakano, T. 1993, *PASJ*, 45, 551
- Nakamura, F., & Umemura, M. 1999a, *ApJ*, 515, 239 (Paper I)
- Nakamura, F., & Umemura, M. 1999b, in *Star Formation 1999*, ed. T. Nakamoto, Nobeyama Radio Observatory, p. 28
- Nakamura, F., & Umemura, M. 2000, in *The First Stars*, eds. A. Weiss, T. Abel, & V. Hill, Springer, p. 263
- Nakamura, F., & Umemura, M. 2001, *ApJ*, 548, 19 (Paper II)
- Nakamura, F., & Umemura, M. 2002, in *New Quest in Stellar Astrophysics: The Link between Stars and Cosmology*, ed. D. Mayya, (Kluwer) in press (astro-ph/0106009)
- Nakamura, T., Umeda, H., Iwamoto, K., Nomoto, K., Hashimoto, M., Hix, W. R., & Thielemann, F.-K. 2001, submitted to *ApJ*, (astro-ph/0011184)
- Nishi, R., Susa, H., Uehara, H., Yamada, M., & Omukai, K. 1998, *Prog. Theor. Phys.*, 100, 881
- Nishi, R., & Tashiro, M. 2000, *ApJ*, 537, 50
- O'Meara, J. M., Tytler, D., Kirkman, D., Suzuki, N., Prochaska, J. X., Lubin, D., & Wolfe, A. M. 2001, accepted by *ApJ*(astro-ph/111790)
- Omukai, K., & Nishi, R., 1998, *ApJ*, 508, 141
- Omukai, K. 2000, *ApJ*, 534, 809
- Palla, F., Salpeter, E. E., & Stahler, S. W., 1983, *ApJ*, 271, 632
- Pustilnik, S. A., Brinks, E., Thuan, T. X., Lipovetsky, V. A., & Izotov, Y. I. 2001, *AJ*, 121, 1413
- Puy, D., & Signore, M., 1996, *A&A*, 305, 371
- Schaerer, D. 2001, submitted to *A&A*
- Shapiro, P. R., & Kang, H. 1987, *ApJ*, 318, 32
- Silk, J. 1977, *ApJ*, 214, 152
- Stancil, P. C., Lepp, S. & Dalgarno, A. 1998, *ApJ*, 509, 1
- Susa, H., & Umemura, M. 2000, *ApJ*, 537, 578
- Tegmark, M., Silk, J., Rees, M., Blanchard, A., Abel, T., & Palla, F. 1997, *ApJ*, 474, 1
- Tsuru, T. G., Awaki, H., Koyama, K., & Ptak, A. 1997, *PASJ*, 49, 619
- Tytler, D., Fan, X.-M., & Burles, S. 1996, *Nature*, 381, 207
- Yoneyama, T. 1972, *PASJ*, 24, 87
- Yoshii, Y., & Sabano, Y. 1980, *PASJ*, 32, 229
- Yoshii, Y., & Saio 1986, *ApJ*, 301, 587
- Uehara, H., Susa, H., Nishi, R., & Yamada, M. 1996, *ApJ*, 473, L95
- Uehara, H., & Inutsuka, S. 2000, *ApJ*, 531, L91
- Umeda, H., & Nomoto, K. 2001, *ApJ*, in press (astro-ph/0103241)
- Umemura, M. 1993, *ApJ*, 406, 361
- Zepf, S. E. & Silk, J. 1996, *ApJ*, 466, 114

TABLE 1
REACTION RATE COEFFICIENTS

Reactions	Rate Coefficients (cm ³ s ⁻¹)	Reference
(D1) $D^+ + e \rightarrow D + h\nu$	$k_{D1} = 3.6 \times 10^{-12} (T/300)^{-0.75}$	SLD98
(D2) $D + H^+ \rightarrow D^+ + H$	$k_{D2} = 3.7 \times 10^{-10} T^{0.28} \exp(-43/T)$	GP98
(D3) $D^+ + H \rightarrow D + H^+$	$k_{D3} = 3.7 \times 10^{-10} T^{0.28}$	GP98
(D4) $D + H \rightarrow HD + h\nu$	$k_{D4} = 1.0 \times 10^{-25}$	GP98
(D5) $D + H_2 \rightarrow H + HD$	$k_{D5} = 9.0 \times 10^{-11} \exp(-3876/T)$	GP98
(D6) $HD^+ + H \rightarrow H^+ + HD$	$k_{D6} = 6.4 \times 10^{-10}$	GP98
(D7) $D^+ + H_2 \rightarrow H^+ + HD$	$k_{D7} = 2.1 \times 10^{-9}$	GP98
(D8) $HD + H \rightarrow H_2 + D$	$k_{D8} = 3.2 \times 10^{-11} \exp(-3624/T)$	GP98
(D9) $HD + H^+ \rightarrow H_2 + D^+$	$k_{D9} = 1.0 \times 10^{-9} \exp(-464/T)$	GP98
(D10) $D + H^+ \rightarrow HD^+ + h\nu$	$k_{D10} = \text{dex}[-19.38 - 1.523 \log T + 1.118(\log T)^2 - 0.1269(\log T)^3]$	GP98
(D11) $D^+ + H \rightarrow HD^+ + h\nu$	$k_{D11} = \text{dex}[-19.38 - 1.523 \log T + 1.118(\log T)^2 - 0.1269(\log T)^3]$	GP98
(D12) $HD^+ + e \rightarrow H + D$	$k_{D12} = 7.2 \times 10^{-8} T^{-1/2}$	GP98
(D13) $D + e \rightarrow D^- + h\nu$	$k_{D13} = 3.0 \times 10^{-16} (T/300)^{0.95} \exp(-T/9320)$	SLD98
(D14) $D^+ + D^- \rightarrow 2D$	$k_{D14} = 5.7 \times 10^{-8} (T/300)^{-0.5}$	SLD98
(D15) $H^+ + D^- \rightarrow D + H$	$k_{D15} = 4.6 \times 10^{-8} (T/300)^{-0.5}$	SLD98
(D16) $H^- + D \rightarrow H + D^-$	$k_{D16} = 6.4 \times 10^{-9} (T/300)^{0.41}$	SLD98
(D17) $D^- + H \rightarrow D + H^-$	$k_{D17} = 6.4 \times 10^{-9} (T/300)^{0.41}$	SLD98
(D18) $D^- + H \rightarrow HD + e$	$k_{D18} = 1.5 \times 10^{-9} (T/300)^{-0.1}$	SLD98

Note. — GP98: Galli & Palla (1998); SLD98: Stancil, Lepp, & Dalgarno (1998)

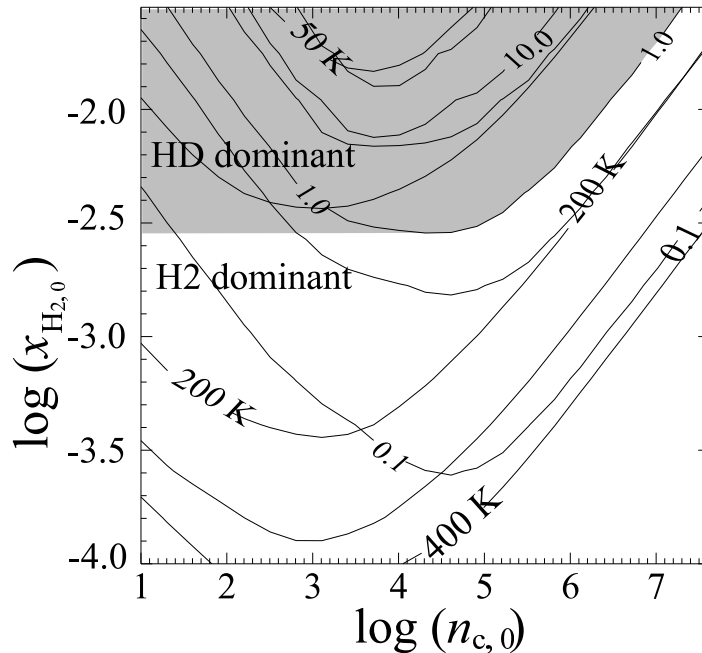


FIG. 1.— Comparison between the HD cooling rate and H₂ cooling rate. The figure shows the HD-to-H₂ cooling ratio in the initial gas density ($n_{c,0}$) – initial H₂ abundance ($x_{\text{H}_2,0}$) diagram. The HD abundance is assumed to be 1×10^{-4} times the H₂ abundance. The solid lines show the contour curves of the HD-to-H₂ cooling ratio, where the equilibrium gas temperatures are determined by the condition of $t_{\text{frag}} = t_{\text{cool}}$ and are indicated by dashed lines. If the initial parameters of the filaments are in the gray region, the HD cooling plays an important role in the thermal evolution of the gas (see the text for more details).

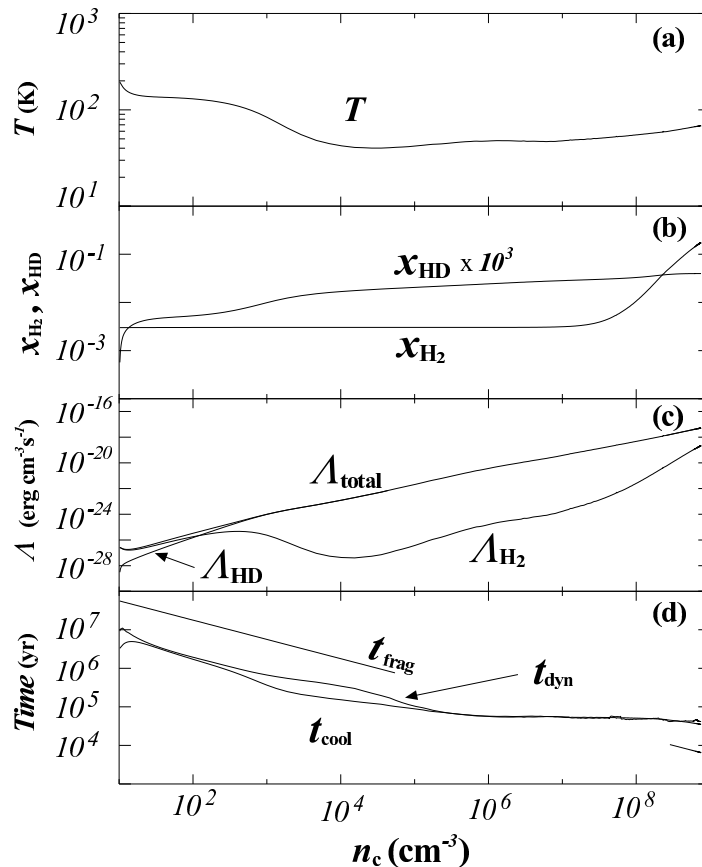


FIG. 2.— Evolution of (a) the temperature, (b) H₂ (solid line) and HD (dashed line) abundances, (c) total (solid line), H₂ (dashed line), and HD (dotted line) cooling rates, (d) the cooling time (solid line), the contraction time (dashed line), and the fragmentation time (dotted line), respectively, as a function of the central density [$n_c \equiv \rho_c / (\mu m_H)$] for the model with $(n_{c,0}, T_0, f, x_{\text{H}_2,0}) = (10 \text{ cm}^{-3}, 200 \text{ K}, 2, 3 \times 10^{-3})$. Note that the definition of the fragmentation time is 2.5 times larger than that in Paper II.

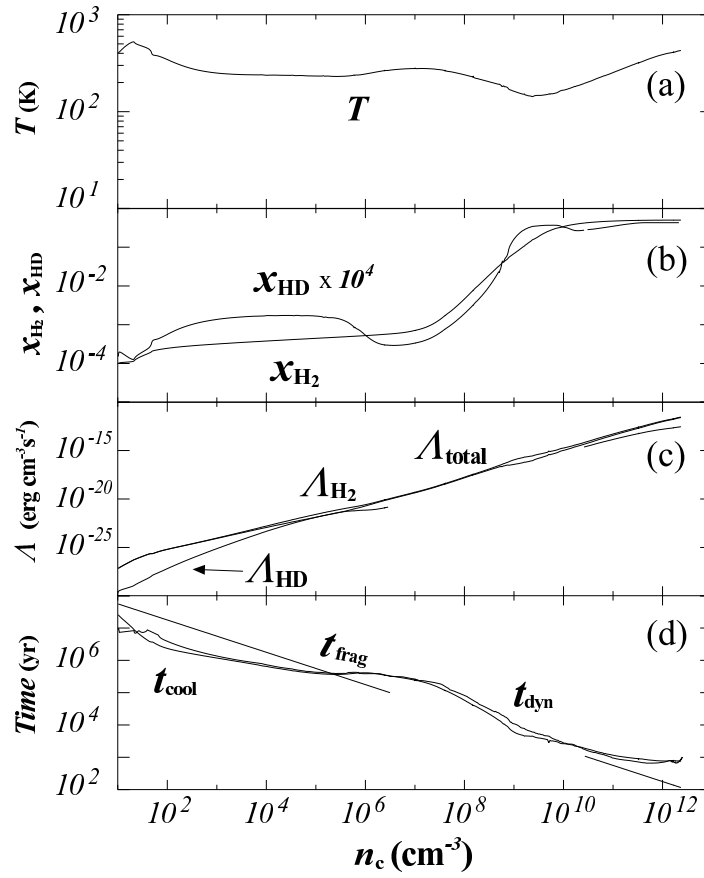


FIG. 3.— Same as Figure 2 but for the model with $(n_{c,0}, T_0, f, x_{\text{H}_2,0}) = (10 \text{ cm}^{-3}, 400 \text{ K}, 2, 1 \times 10^{-4})$.

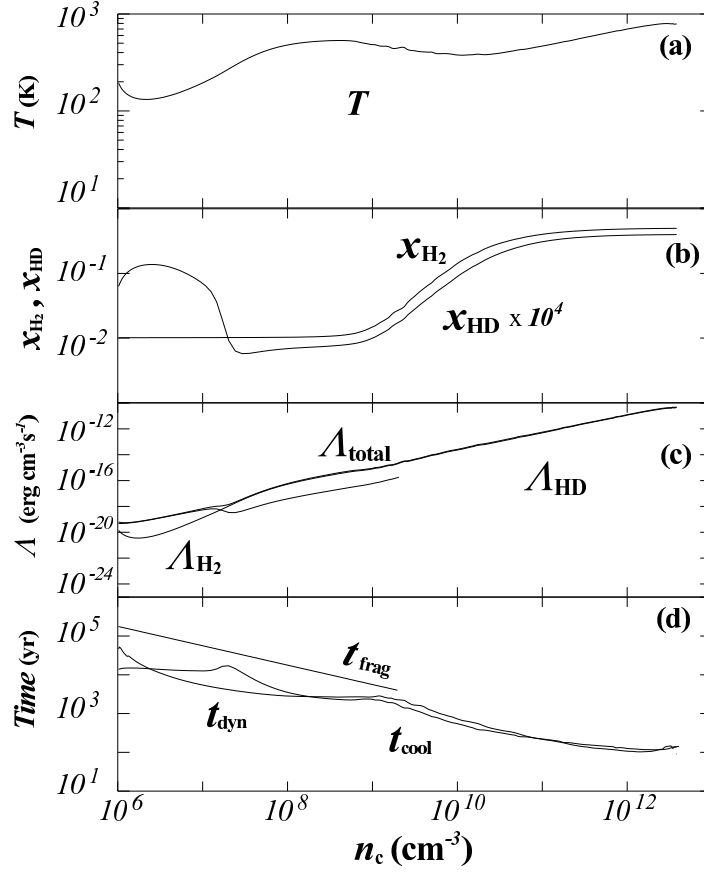


FIG. 4.— Same as Figure 2 but for the model with $(n_{c,0}, T_0, f, x_{\text{H}_2,0}) = (10^6 \text{ cm}^{-3}, 200 \text{ K}, 6, 1 \times 10^{-2})$.

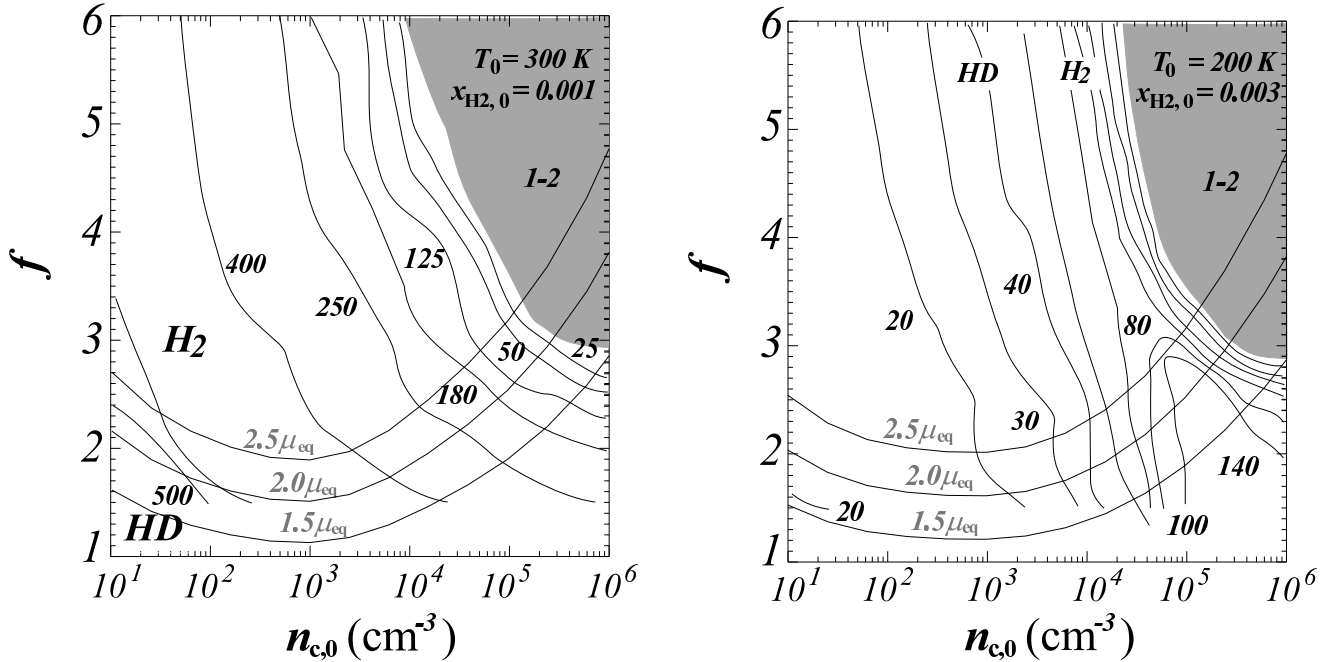


FIG. 5.— The distributions of fragment mass for the models with (a) $T_0 = 300 \text{ K}$ and $x_{\text{H}_2,0} = 1 \times 10^{-3}$ and (b) $T_0 = 200 \text{ K}$ and $x_{\text{H}_2,0} = 3 \times 10^{-3}$. (T_0 is close to the equilibrium temperature for each value of $x_{\text{H}_2,0}$.) The abscissa and ordinate denote the initial central density and the parameter f , respectively. The solid lines denote the contours of the fragment mass which are labeled with adjacent numbers in units of M_\odot . A thick dashed line shows the lines at which $\Lambda_{\text{HD}} = \Lambda_{\text{H}_2}$ at the epoch of fragmentation. In the left regions of the dashed lines, HD cooling is more efficient than H_2 cooling. The dot-dashed lines show the line masses of the filaments formed by fragmentation of self-gravitating gas disks (see the text for more details), where μ_{eq} is a line mass of an equilibrium filament. The number attached by each line denotes the line mass in units of μ_{eq} .